Running title: A novel neurological mutant in rats caused by the myosin Va gene

Myosin Va mutation in rats is an animal model for the human hereditary neurological disease, Griscelli syndrome type 1

Yoshiko Takagishi and Yoshiharu Murata

Department of Genetics, Division of Stress Adaptation and Protection, Research Institute of Environmental Medicine, Nagoya University, Nagoya 464-8601, Japan

Address for correspondence: Yoshiko Takagishi, Ph. D., Research Institute of Environmental Medicine, Nagoya University, Furo-cho, Chikusa-ku, Nagoya 464-8601, Japan, Phone: +81-52-789-3874; Fax: +81-52-789-3876
E-mail: taka@riem.nagoya-u.ac.jp

Key words: mutant; cerebellum; smooth endoplasmic reticulum; Purkinje cells; calcium; synaptic plasticity

Abstract

A spontaneous neurological mutation, *dilute-opisthotonus (dop),* was discovered in our breeding colony of Wistar rats. We found that the mutation affected the gene encoding Myosin Va (MyoVA), an actin-based molecular motor. Analysis of the myosin Va (*Myo5a)* gene of the *dop* genome showed the presence of a complex rearrangement consisting of a 306-bp inversion associated with 217-bp and 17-bp deletions. A 141 bp exon is skipped in the *dop* transcript, producing a *dop* cDNA with a 141 in-frame deletion in the sequences encoding the head region. Expression of the MyoVA protein is severely impaired in the brains of *dop* homozygous rats, suggesting they have a null mutation for *Myo5a*. In a morphological analysis of the cerebella of *dop* rats, we found an absence of smooth endoplasmic reticulum (SER) and of inositol 1,4,5-triphosphate (IP3) receptors in the dendritic spines of Purkinje cells (PC). The SER acts as an intracellular Ca^{2+} store and IP3-mediated Ca^{2+} signaling in dendritic spines plays a critical role in synaptic regulation. We therefore measured synaptic transmission and long-term depression (LTD), a form of synaptic plasticity underlying cerebellar motor learning, at PC synapses in the cerebella of *dop* rats. We found that synaptic transmission at the PC synapses is largely normal, while the LTD is deficient due to a decrease in IP3-mediated Ca^{2+} release from the SER in the PC spines of the *dop* cerebella. These findings may account for the ataxic movements and clonic convulsions displayed by *dop* rats. They also contribute to our understanding of the neurological disease mechanisms of the human hereditary disease Griscelli syndrome type 1, which is caused by mutation of the *MYO5A* gene.

Introduction

Spontaneous mutants provide valuable animal models for investigating the underlying pathogenesis and disease mechanisms of human inherited neurological disorders. Furthermore, the study of these model organisms can provide important insights into how genes regulate the development and function of the nervous system. More than 100 mutant genes associated with neurological disorders have been reported in mice. [1] However, fewer such genes are known in rats. Here we describe a novel spontaneous rat mutant that displays neurological disease. We also describe the mutational changes in the affected gene (myosin Va; *Myo5a*) and review our analyses of the morphology and function of the cerebellum of mutant rats. [2-5] These studies contribute to our understanding of the human hereditary neurological disease Griscelli syndrome type 1, which is caused by mutation of the myosin Va (*MYO5A*) gene (GS1:OMIM 214450).

Ataxic rats were found in a breeding colony of Wistar rats and the abnormal phenotype was shown to be controlled by an autosomal recessive gene. [6] On a pigmented background, mutant homozygotes are distinguishable from their normal littermates at 3~4 days of age by their lighter pigmentation and their subsequent diluted coat color. After 11 days of age, they develop movement disorders such as staggering and difficulty in walking. Around 14~16 days, the symptoms become more severe and mutants manifest clonic convulsion with opisthotonus (Fig.1). Finally, they die at 21~22 days of age, probably due to difficulties of food and water intake. On the basis of this phenotype, we named the mutation *dilute-opisthotonus*, with the gene symbol *dop*. Currently, the *dop*

mutation is maintained in the DOP rat strain. Linkage analysis using PCR-amplified microsatellite markers showed that the *dop* mutation mapped to a locus on chromosome 8. [7] Rat chromosome 8 shows conserved homology to mouse chromosome 9 and gene order in the two species is well conserved across many chromosomal segments. Comparison of the genetic maps of rat chromosome 8 and mouse chromosome 9 indicates that the *dop* locus may be homologous to the mouse *dilute* locus . [7]

Identification of the *dop* gene

The mouse *dilute* locus encodes an actin based molecular motor, Myosin Va (MyoVA). [8] More than 200 alleles have been identified at the *dilute* locus; homozygotes of two of these alleles, *dilute-lethal* (*d-l/d-l*) and *dilute-lethal*^{20J} (*d-l*^{20J}/*d-l*^{20J}), exhibit a similar phenotype, diluted coat color and neurological disorders, to that of the rat *dop* mutant. [9] Analyses have shown that the *d-l*^{20J} allele has a deletion in the *Myo5a* gene that results in a markedly reduced expression level of the transcript and a complete absence of the MyoVA protein. [10]

The evidence from studies of *dilute* mutations in the mouse suggested that the *dop* mutation affects the homologous locus in rats. We therefore cloned and characterized the *Myo5a* cDNA from wild-type and *dop* rats. Wild-type rat *Myo5a* cDNA obtained from brain tissue was amplified by RT-PCR with primers designed using the mouse *Myo5a* cDNA sequence. [8] The wild-type rat cDNA was sequenced and found to contain a 5487-bp ORF, encoding 1829 amino acids (Fig. 2 in ref 2). The deduced amino acids sequence showed 97%, 96%, and 90% identity with mouse MyoVA, [8] human MYH12, [11]

and chicken p190, [12] respectively. [2] Next we cloned and sequenced *dop Myo5a* cDNA obtained from brain tissue. We found that this cDNA had a 141-bp deletion (from position 1442 to 1582) in the head region (Fig. 2A, B). The deletion, designated Δ1442-1582, removes 47 amino acids (residues 468–514) without disrupting the ORF (Fig. 2A). This deletion was the only sequence difference between the wild-type and the *dop* cDNAs.

To investigate further the nature of the *dop* gene mutation, we used primers for sequences flanking the 1442-1582 cDNA segment to amplify this region from genomic DNA. From wild-type DNA, a fragment of approximately 5 kb was recovered. This fragment contains a single exon, encoding the region 1442-1582, that is preceded by a 3.0 kb intronic sequence and followed by a 1.5 kb intron (Fig. 2C). Genomic DNA from *dop* rats also yielded a fragment of approximately 5 kb. Sequence analysis revealed that the fragment contained a complex rearrangement consisting of a 306-bp inversion associated with 217-bp and 17-bp deletions.

Expression of Myo5a mRNA and the MyoVA protein in the dop brain.

Next we asked whether the *dop* mutation affects expression of *Myo5a* mRNA and of the MyoVA protein. First, total RNAs were extracted from the brains of both normal and *dop* rats at 2 weeks of age. Brain mRNA was hybridized with mouse *Myo5a* cDNA. [8] Three major transcripts were observed in both the control and the *dop* mRNAs (Fig.1 in ref 2). These three transcripts have also been detected in mice. [8] No obvious differences in size were detected between the control and *dop* transcripts.

Expression of the MyoVA protein was examined by Western blot analysis using antibodies against the tail domain of MyoVA. [12] Total proteins were extracted from the cerebrum and cerebellum of both normal and *dop* rats aged 2~3 weeks. The proteins were then used for immunoblotting. MyoVA was detected as a single band of the expected molecular mass of 190 kDa in the sample from the normal cerebrum and cerebellum. However, no bands were found in proteins extracted from *dop* brains (Fig. 3), indicating that MyoVA expression is severely impaired in the *dop* brain. We conclude, therefore, that the *dop* rats carry a null mutation for the *Myo5a* gene.

Morphological study of the cerebellum from myosin Va null mutants

On the basis of the initial neurological symptom of ataxia in mutant rats, we investigated cerebellar morphology in *dop* rats aged 18~22 days. We also performed a similar analysis in *Myo5a* null, *dilute-lethal (d-l)* homozygous mice. Although the brains of mutant animals were slightly smaller than those of their normal littermates, the cerebella of mutant and normal animals were indistinguishable with respect to gross anatomy (Fig. 4A). Foliation was well developed and cortical organization was well established in the cerebella of mutants (Fig. 4B). The neurons in each cortical layer appeared normal and there was no obvious indication of loss of Purkinje cells or of granule cells (Fig. 4C).

We performed immunohistochemistry with antibodies for calbindin D-28k (CD-28k) and inositol-1,4,5-trisphosphate (IP3) receptors to examine the neuronal differentiation of Purkinje cells (PCs). Both proteins are highly expressed in PCs. [13-15] At low magnification, PCs of mutant animals had round somata and well developed

dendrites (Fig. 5A-C). At higher magnification, however, IP3 receptors appeared to be sparse in distal dendrites compared to the staining of CD-28k in the dendrites (Fig. 5H). In normal rats and mice, the distribution of both proteins overlapped throughout the soma, proximal and distal dendrites, and the spines (Fig. 5D-F). In contrast, no overlap was present in the PC spines of *dop* rats (Fig. 5G-I) or of *d-l* mice (data not shown). [4, 5] These findings indicate that IP3 receptors are absent from PC spines in the *Myo5a* null mutants, *dop* rats and *d-l* mice.

We examined the ultrastructure of the dendritic spines of PCs by electron microscopy. A large number of synapses between PC spines and parallel fibers (PFs) were formed in the neuropile of the molecular layer of both normal and mutant cerebella. In normal rats and mice, the PC spines contained small tubular elements, i.e. smooth endoplasmic reticulum (SER) (Fig. 6A, arrows). In contrast, no SER was found in the filamentous matrix of the PC spines of mutants (Fig. 6B), although it was present in the dendrites and the somata (Fig. 6B). SER never penetrated from the dendrites into the PC spines of mutants (Fig. 6B, inset) but did so in normal PCs (Fig.6A, inset). The synapses between PC spines and PFs appeared normal in terms of conspicuous pre- and post-synaptic membrane densities and clustering of synaptic vesicles near the presynaptic membranes. The number of PF synapses per 100 μm^2 of molecular layer was 10.9 ± 2.5 (n = 12) for *dop* mutants and 13.7 ± 2.1 (n = 10) for normal rats, showing no significant difference ($p > 0.05$, Mann-Whitney U test). [5] Overall, our studies of the morphology of the cerebellum have shown that the *Myo5a* null mutation causes absence of SER and IP3 receptors in PC spines. [3, 4] The SER is an extensive and highly interconnected membrane

system in neuronal cells[16, 17]; the SER in PC spines may mark an end portion of this membranous system. Our observations here suggest that MyoVA may be involved in the membrane transport function of SER from the dendrites of PCs into the spines, where actin is rich.

Functional analysis of the cerebellum of myosin Va null mutants

We addressed the question of whether the *Myo5a* null mutation affects synaptic transmission in mutant cerebella. For this purpose, we used whole-cell patch clamp recording from PC somata in parasagittal slices and measured excitatory postsynaptic currents (EPSCs) resulting from selective stimulation of PFs or climbing fibers (CFs). [5] In control and mutant (*dop* and *d-l*) rats and mice, PF stimulation evoked EPSCs whose amplitudes varied with stimulus intensity. There was no significant difference between control and mutant animals in the kinetics of PF-mediated EPSCs. [5] Moreover, PF-EPSCs were facilitated in response to a second stimulus at interpulse intervals between 10 and 300 ms in both controls and mutants (Fig. 4B in ref 5). This paired-pulse facilitation depends on the amount of neurotransmitter released from presynaptic terminals, so the lack of effect on facilitation suggests that transmitter release is normal at the PF synapses of mutants.

At the CF synapses of both controls and mutants, stimulation induced large EPSCs with one or, occasionally, multiple discrete steps. This indicates that the incidence of multiple innervation was unchanged in the mutants compared to the controls. There was no significant difference in either the rise times or decay time constants of CF-EPSCs. [5]

CF-EPSCs exhibited paired-pulse depression at interpulse intervals between 50 and 3000 ms, due mainly to decreased transmitter release in response to the second pulse. The magnitude of paired-pulse depression tended to be greater in mutants than in normal littermates, especially at brief inter-pulse intervals (Fig. 4D in ref 5). This suggests a slight change in neurotransmitter release and/or a retardation of development at the mutant CF synapse. These results indicate that the *Myo5a* null mutation has little effect on synaptic transmission at CF synapses. Voltage-gated Ca^{2+} currents of mutant PCs were similar in their amplitudes and kinetics as well as their voltage dependence when compared to those recorded from PCs of control rats. [5] Overall, our findings indicate that synaptic transmission is largely normal in *Myo5a* null mutant cerebella.

Next we asked whether the mislocalization of SER and IP3 receptors in PC spines affects long-term synaptic depression (LTD), a form of synaptic plasticity underlying motor learning in the cerebellum. [18] Many lines of evidence point toward a central role for postsynaptic Ca^{2+} in the induction of LTD and it has been proposed that Ca^{2+} release from intracellular stores via IP3 receptors is essential for LTD. [18-20] We examined LTD in PF-PC synapses of cerebella from *dop* rats and *d-l* mice. LTD was induced by simultaneous activation (1 Hz for 5 min) of PF and CF synapses (Fig. 7A, C left), in accordance with a protocol that is optimal for inducing LTD. [21] At 30 min after the onset of this stimulation, the mean slope of excitatory postsynaptic potentials (EPSPs) resulting from PF activity was depressed by 28.8% $\pm$8.6% (mean $\pm$ SEM; n = 10) of the control value measured prior to pairing. In contrast, in *dop* mutant rats, the same combination of PF and CF stimulation did not induce LTD (Fig. 7B, C right). The mean value of the

EPSP slope was not depressed (4.1% $\pm$ 7.0% increase; n = 9) when measured 30 min after paired synaptic activity. The difference between these two values is significant ($p < 0.005$). LTD was also absent in *d-l* mutant mice (Fig. 7D). Thus the cerebellar LTD was clearly deficient in the *Myo5a* null mutants and we suggest that the LTD deficiency is as a result of the absence of IP3-sensitive Ca^{2+} stores in PC spines, i.e. a lack of Ca^{2+} release from the SER in the PC spines of mutants.

We measured Ca^{2+} signals in PC spines to determine whether impairment of IP3-mediated Ca^{2+} signaling accounts for the LTD lesion. PFs were repetitively stimulated (80 Hz, 200 ms) and the resulting Ca^{2+} signals were measured in PC dendritic spines and shafts. [22] In both control and mutant rats, PF activity caused transient rises in postsynaptic Ca^{2+} concentration (Fig. 8A). However, these Ca^{2+} signals were significantly smaller in mutants than in controls. The postsynaptic Ca^{2+} signal arises from two sources: Ca^{2+} influx, and IP3-mediated release of Ca^{2+} from intracellular stores. [19, 20] When IP3-mediated release of Ca^{2+} from intracellular stores was separated from Ca^{2+} influx, the IP3-mediated components were smaller in both the dendritic spines and adjacent shafts (Fig. 8B). This decrease in IP3-mediated Ca^{2+} release in the PC spines is consistent with the absence of SER and IP3 receptors in the spines in mutants. Taken together, our findings suggest that Ca^{2+} release from the SER in PC spines is not essential for basic synaptic transmission but is of crucial importance for the induction of synaptic plasticity.

Human inherited disease caused by the myosin Va gene: concluding remarks

Class V myosin is a well-characterized unconventional myosin heavy chain and, in vertebrates, has the subclasses Va, Vb and Vc. [23] Myosin Va is the predominant neuronal type and is highly expressed in the brain; it also shows expression in the skin. [8, 12] It has been established that MyoVA functions in organelle transport and membrane trafficking. [24-26] Thus, the loss of MyoVA function in mutant rats and mice would be expected to have a phenotypically deleterious effect. Indeed, the diluted coat color of mutants is the result of a defect of melanosome transport on actin filament to dock at plasma membrane and a failure of their release into keratinocytes. [27, 28] MyoVA has been proposed to function in axonal and dendritic transport, [24, 25, 29] however, the specific roles of the protein in neurons have yet to be determined.

In humans, the *MYO5A* gene mutation causes an autosomal recessive genetic disorder, Griscelli syndrome type 1 (GS1: OMIM 214450). The human *MYO5A* gene is located on chromosome 15q21. GS1 is characterized by partial albinism and neurological impairment. [30, 31] Patients exhibit pigmentary dilution in their skin and hair and develop hypotonia, marked motor developmental delay and mental retardation. [30, 31] It has been suggested that Elejalde syndrome (OMIM 256710), neuroectodermal melanolysosomal syndrome, may represent the same entity as GS1. [32, 33] Another form of Griscelli syndrome, type 2 (GS2: OMIM 607624) is caused by mutation in the *RAB27A* gene, which encodes a small GTPase protein, Rab 27A, that is involved in the regulation of the intracellular secretion pathway. The phenotype is similar to GS1: patients manifest hypopigmentation of the skin and hair and occasionally neurological defects.

Furthermore, the mutation is associated with a cytotoxic defect and uncontrolled T-lymphocytes and macrophage–activation known as hemophagocytotic syndrome. Patients with GS1, however, never develop hemophagocytotic syndrome. The *MYO5A* and *RAB27A* genes are located in the same region of chromosome 15q21 and are separated by less than 1.6 cM. [34] Melanosome transport requires the interaction of MyoVA and Rab27a via the Rab27a effector (melanophilin) that interacts specifically with an alternatively spliced exon F in the myosin Va gene. [35] However, this protein complex has not been identified to date in the brain. Brain-specific exon B in the myosin Va gene [36] may interact with the Rab effector for another Rab GTPase. Determination of the function and properties of MyoVA in the brain will be essential for a more complete understanding of the neurological pathogenesis and disease mechanism of GS1. Characterization of spontaneous myosin Va mutants will undoubtedly be of considerable value in this endeavor. As we have described here, the absence of SER from the PC spines of *Myo5* null mutants causes impairment of IP3-mediated Ca^{2+} release, resulting in a defect of LTD underlying cerebellar motor learning. In part at least, these findings explain the root of the neuronal defect of GS1. We are undertaking further studies to elucidate the specific roles of MyoVA in particular areas of the brain, with the aim of understanding the disease mechanisms that underlie the neurological phenotypes of animals and humans with myosin Va mutations.

Acknowledgments.

This study was supported by grants from the Japanese Ministry of Education, Science,

Sports and Culture (Grant-in-Aid No. 0760708) and from the Nagoya University Foundation (to Y.T.). Figures 7 and 8 are reprinted from Neuron, vol.28, Miyata M, Finch EA, Khiroug L, Hashimoto K, Hayasaka S, Oda S, Inouye M, Takagishi Y, Augustine GJ, Kano M. Local calcium release in dendritic spines required for long-term synaptic depression. 233-244, Copyright (2000) with permission from Elsevier.

References

1. Green, M.C. 1989. Catalog of mutatn genes and polymorphic loci. *In* Genetic variants and strains of the laboratory mouse. M.F. Lyon & A.G. Searle, eds.: 12-403. Gustav Fischer Verlag. New York

2. Futaki, S.*, et al.* 2000. Identification of a novel myosin-Va mutation in an ataxic mutant rat, *dilute-opisthotonus.* Mamm. Genome. **11**: 649-655.

3. Dekker-Ohno, K.*, et al.* 1996. Endoplasmic reticulum is missing in dendritic spines of Purkinje cells of the ataxic mutant rat. Brain Res. **714**: 226-230.

4. Takagishi, Y.*, et al.* 1996. The *dilute-lethal (dl)* gene attacks a Ca^{2+} store in the dendritic spine of Purkinje cells in mice. Neurosci. Lett. **215**: 169-172.

5. Miyata, M.*, et al.* 2000. Local calcium release in dendritic spines required for long-term synaptic depression. Neuron. **28**: 233-244.

6. Dekker-Ohno, K.*, et al.* 1993. An ataxic mutant rat with dilute coat color. Lab. Anim. Sci. **43**: 370-372.

7. Ohno, K.*, et al.* 1996. Mapping of the *dilute-opisthotonus* (*dop*) gene on chromosome 8 of the rat. Exp. Anim. **45**: 71-75.

8. Mercer, J. A.*, et al.* 1991. Novel myosin heavy chain encoded by murine *dilute* coat color locus. Nature. **349**: 709-713.

9. Searle, A., G. 1952. A lethal allele of dilute in the house mouse. Heredity. **6**: 395-401.

10. Strobel, M. C.*, et al.* 1990. Molecular analysis of two mouse dilute locus deletion mutations: spontaneous dilute lethal^{20J} and radiation-induced dilute prenatal lethal Aa2 alleles. Mol. Cell Biol. **10**: 501-509.

11. Lambert, J.*, et al.* 1998. Myosin V colocalizes with melanosomes and subcortical actin bundles not associated with stress fibers in human epidermal melanocytes. J. Invest. Dermatol. **111**: 835-840.

12. Espreafico, E. M.*, et al.* 1992. Primary structure and cellular localization of chicken brain myosin-V (p190), an unconventional myosin with calmodulin light chains. J. Cell Biol. **119**: 1541-1557.

13. de Talamoni, N.*, et al.* 1993. Immunocytochemical localization of the plasma membrane calcium pump, calbindin-D28k, and parvalbumin in Purkinje cells of avian

and mammalian cerebellum. Proc. Natl. Acad. Sci. U S A. **90**: 11949-11953.

14. Maeda, N., *et al.* 1989. Developmental expression and intracellular location of P400 protein characteristic of Purkinje cells in the mouse cerebellum. Dev. Biol. **133**: 67-76.

15. Ross, C. A., *et al.* 1989. Inositol 1,4,5-trisphosphate receptor localized to endoplasmic reticulum in cerebellar Purkinje neurons. Nature. **339**: 468-470.

16. Martone, M. E., *et al.* 1993. Three-dimensional visualization of the smooth endoplasmic reticulum in Purkinje cell dendrites. J. Neurosci. **13**: 4636-4646.

17. Levine, T. & C. Rabouille. 2005. Endoplasmic reticulum: one continuous network compartmentalized by extrinsic cues. Curr. Opin. Cell Biol. **17**: 362-368.

18. Ito, M. 2001. Cerebellar long-term depression: characterization, signal transduction, and functional roles. Physiol. Rev. **81**: 1143-1195.

19. Augustine, G. J., F. Santamaria & K. Tanaka. 2003. Local calcium signaling in neurons. Neuron. **40**: 331-346.

20. Hartmann, J. & A. Konnerth. 2005. Determinants of postsynaptic Ca^{2+} signaling in Purkinje neurons. Cell Calcium. **37**: 459-466.

21. Miyata, M., *et al.* 1999. Corticotropin-releasing factor plays a permissive role in cerebellar long-term depression. Neuron. **22**: 763-775.

22. Finch, E. A. & G. J. Augustine. 1998. Local calcium signalling by inositol-1,4,5-trisphosphate in Purkinje cell dendrites. Nature. **396**: 753-756.

23. Berg, J. S., B. C. Powell & R. E. Cheney. 2001. A millennial myosin census. Mol. Biol. Cell. **12**: 780-794.

24. Bridgman, P. C. 2004. Myosin-dependent transport in neurons. J. Neurobiol. **58**: 164-174.

25. Bridgman, P. C. & L. L. Elkin. 2000. Axonal myosins. J Neurocytol. **29**: 831-841.

26. Reck-Peterson, S. L., *et al.* 2000. Class V myosins. Biochim. Biophys. Acta. **1496**: 36-51.

27. Provance, D. W., Jr., *et al.* 1996. Cultured melanocytes from dilute mutant mice exhibit dendritic morphology and altered melanosome distribution. Proc. Natl. Acad. Sci. U S A. **93**: 14554-14558.

28. Wu, X., *et al.* 1997. Myosin V associates with melanosomes in mouse melanocytes: evidence that myosin V is an organelle motor. J. Cell Sci. **110**: 847-859.

29. Langford, G. M. & B. J. Molyneaux. 1998. Myosin V in the brain: mutations lead to neurological defects. Brain Res. Rev. **28**: 1-8.

30. Pastural, E., *et al.* 1997. Griscelli disease maps to chromosome 15q21 and is associated with mutations in the myosin-Va gene. Nat. Genet. **16**: 289-292.

31. Menasche, G., *et al.* 2003. Griscelli syndrome restricted to hypopigmentation results from a melanophilin defect (GS3) or a MYO5A F-exon deletion (GS1). J. Clin. Invest. **112**: 450-456.

32. Ivanovich, J., *et al.* 2001. 12-year-old male with Elejalde syndrome (neuroectodermal melanolysosomal disease). Am. J. Med. Genet. **98**: 313-316.

33. Duran-McKinster, C., *et al.* 1999. Elejalde syndrome-a melanolysosomal neurocutaneous syndrome: clinical and morphological findings in 7 patients. Arch. Dermatol. **135**: 182-186.

34. Menasche, G., *et al.* 2000. Mutations in RAB27A cause Griscelli syndrome associated with haemophagocytic syndrome. Nat. Genet. **25**: 173-176.

35. Wu, X. S., *et al.* 2002. Identification of an organelle receptor for myosin-Va. Nat. Cell Biol. **4**: 271-278.

36. Huang, J. D., *et al.* 1998. Molecular genetic dissection of mouse unconventional myosin-VA: head region mutations. Genetics. **148**: 1951-1961.

Figure Legends

Figure 1. *Dilute-opisthotonus* rats at 3 weeks of age.

The *dop/dop* mutant exhibits a diluted coat color compared to a normal rat (left) and the neurological symptoms of opisthotonus and limb convulsions.

Figure 2. Genomic analysis of the *dop* mutation.

A: Partial sequence alignment of the *Myo5a* cDNAs of wild-type (WT) and *dop* rats and the deduced amino acids. The deletion region (nucleotides 1442-1582) in *dop* is indicated by the gap.

B: A schematic diagram of the *Myo5a* cDNA showing the coding region by the open box and the untranslated regions by lines. The 1442–1582 region is indicated as a solid box in the coding region.

C: A schematic presentation of the genomic rearrangement in the *dop* mutation. The genomic structure of the wild type (wild) and the *dop* allele (*dop*) are aligned. Exons are indicated as boxes and introns are indicated as lines. The exon skipped in the *dop* transcript is indicated as a black box. Note that the region containing exon is inverted in the *dop* allele. Gray lines in the *dop* allele indicate its splicing pattern. Small arrows indicate the PCR primers used for the genomic PCR. (Modified from Futaki et al. [2])

Figure 3.

Expression of the Myosin Va protein in the *dop* brain

Protein was extracted from the cerebrum (Cortex) and cerebellum (Cbll) of the normal and *dop* rat brains and was run on a 7.5% SDS-PAGE. The gels were immunoblotted with an anti-Myosin Va antibody. [12] Bands representing the MyoVA protein were detected at approximately 190 kDa in normal rats but not *dop* rats.

Figure 4.

Morphological analysis of the cerebellum of *dop* rats

A: Brains from normal and *dop* rats. The *dop* cerebellum is slightly smaller than that of a normal rat. B: Mid-sagittal planes of the cerebella from normal and *dop* rats. No obvious differences were found in foliation and layer formation between normal (N) and *dop* rats. C: Higher magnification images of the cortical layers of the cerebellum. Neurons in each layer form normally and Purkinje cells align as a monolayer in the *dop* cerebellum. ML: the molecular layer; PL: Purkinje cell layer; GL: the granular layer. Bars: 500 μm in B; 100 μm in C.

Figure 5.

Immunohistochemical analysis of Purkinje cells in *dop* rats

Green (A, D, G): calbindin D-28k (CD-28k) staining, Red (B, E, H): IP3 receptor staining. Yellow (C, F, I): merged. A-C: Lower magnification images from *dop* rats. D-I: Higher magnification images from normal (D-F) and *dop* (G-I) rats. The somata and dendrites of Purkinje cells (PC) are stained with both antibodies for CD-28k and IP3 receptors and, at lower magnifications, show an apparently overlapping distribution of the two proteins. At higher magnification, however, it can be seen that the tips of the distal PC dendrites of the *dop* rat are not stained by the anti-IP3 receptor antibody (H) and that the distribution of the IP3 receptor does not completely overlap CD-28k staining (arrows in I). Bars: 50μm in A; 10μm in D and G

Figure 6.

Electron microscopy of Purkinje cell synapses of *dop* rats.

Numerous Purkinje cell (PC) synapses with parallel fiber (pf) are formed in the molecular layers of normal (A) and *dop* (B) rats. PC spines (S) contain tubular structures, smooth endoplasmic reticulum (SER), in normal rats (arrows in A). The inset shows that the SER in the spine (arrow) seem to be continuous with the SER of the dendrites (PCD) (arrow head). In contrast, PC spines do not contain SER in the *dop* rat (B). SER is present in the PC dendrites (arrow head in B) but do not penetrate into the spine (inset in B) in *dop* rats. Bars: 500 nm.

Figure 7.

Analysis of synaptic plasticity, cerebellar long-term depression (LTD) in myosin Va mutants

A: Traces of parallel fiber (PF)-excitatory postsynaptic potentials (EPSPs) measured in a control rat Purkinje cell before (pre) and 25 min after a combination of PF and CF stimulation. The reduction in the EPSP at the 25 min interval is due to LTD. B: PF-EPSPs measured in a *dop* Purkinje cell, showing an absence of LTD. C: In Purkinje cells from control rats (left), a combination of PF and CF stimulation (horizontal bar) resulted in LTD of the PF-EPSP initial slopes. In Purkinje cells from *dop* mutant rats (right), the combination of PF and CF stimulation did not induce LTD. D: the combined stimulation protocol induced LTD in Purkinje cells from control mice (left) but not *d-l* mutant mice (right). The data in (C) and (D) are pooled and normalized against the mean initial PF-EPSP slope during the control period prior to conditioning. (From Miyata et al. [5]. Reprinted with permission from Elsevier).

Figure 8.

Analysis of Ca^{2+} signals in PC spines evoked by PF activity in myosin Va mutants

A: Pseudocolored Ca^{2+} signals produced by a train of stimuli applied to PFs (200 ms, 80 Hz) of a control (top) and a mutant (center) mouse. The images represent the peaks of the Ca^{2+} signals and are averages of frames acquired 233-500 ms after the onset of PF stimulation. The bottom panel shows a high-magnification image of the area indicated by the dashed box in the middle panel. This image illustrates a spiny dendrite, and the circles indicate representative regions in which shaft (black) and spine (white) Ca^{2+} signals were measured.

B: Ca^{2+} signals produced by PF stimulation (200 ms, 80 Hz, gray bars) in the dendritic spines (top) and shafts (bottom) of a control (left) and a mutant (right) rat. Rows 1 and 4 show the time course of the Ca^{2+} signals obtained in the control solution, and rows 2 and 5 show the Ca^{2+} signals obtained in the presence of the mGluR blocker, 4-CPG, which eliminates the Ca^{2+} signals associated with IP3-mediated Ca^{2+} release from intracellular stores. The difference between these two conditions indicates the component of the Ca^{2+} signal due to Ca^{2+} release mediated by mGluRs (rows 3 and 6). Traces are averages of eight spine/dendrite pairs in the mutant and nine spine/dendrite pairs in the control. Measurements are from different cells than shown in (A). (From Miyata et al. [5]. Reprinted with permission from Elsevier).

Fig.1

Fig.2

A


WT TAGTTTTGAACAGTTCTGCATAAATTATGCAAATGAAAAGCTACAGCAACAATTCAACATGCATGTCTCCAAACTGGAACAGGAGGAGTA 1470
dop TAGTTTTGAACAGTTCTGCATAAATTATGCAAATGAAAAGCTACAGCAACAATTCAACATG----------
S F E Q F C I N Y A N E K L Q Q Q F N M H V S K L E Q E E Y 477
WT CATGAAGGAACAAATTCCATGGACACTCATAGATTTCTATGATAATCAGCCTTGTATCAATCTTATAGAATCTAAACTGGGTATTCTAGA 1560
dop ----------
M K E Q I P W T L I D F Y D N Q P C I N L I E S K L G I L D 507
WT TTTGCTGGATGAGGAATGTAAGATGCCTAAAGGTACCGATGACACATGGGCCCAAAAACTATACAACACACATTTGAACAAATGTGCTCT 1650
dop ----------ATGCCTAAAGGTACCGATGACACATGGGCCCAAAAACTATACAACACACATTTGAACAAATGTGCTCT
L L D E E C K M P K G T D D T W A Q K L Y N T H L N K C A L 537

B

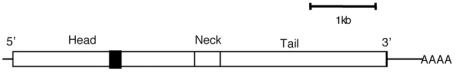
1kb
5'
Head
Neck
Tail
3'
AAAA

C

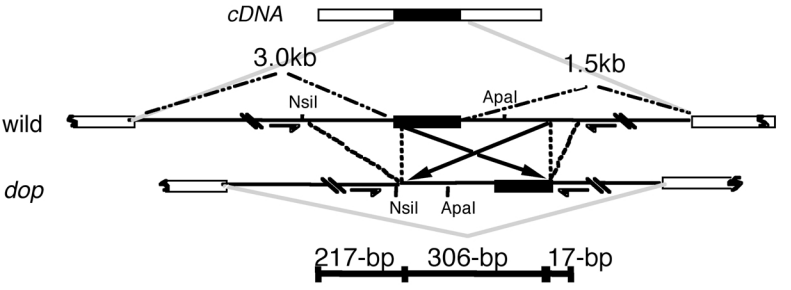
cDNA
3.0kb
1.5kb
NsiI
ApaI
wild
dop
NsiI
ApaI
217-bp
306-bp
17-bp

Fig.3

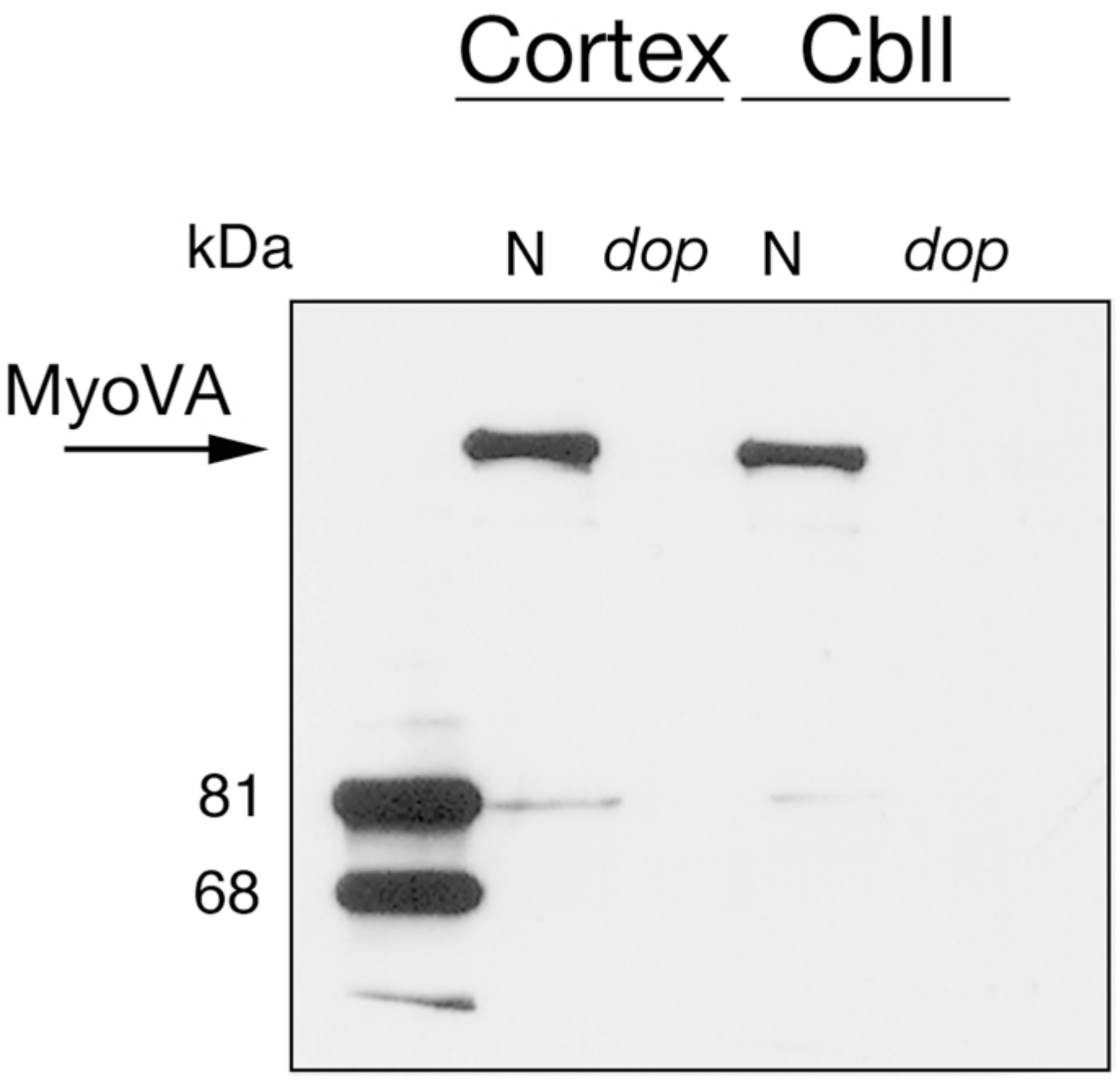

Fig.4

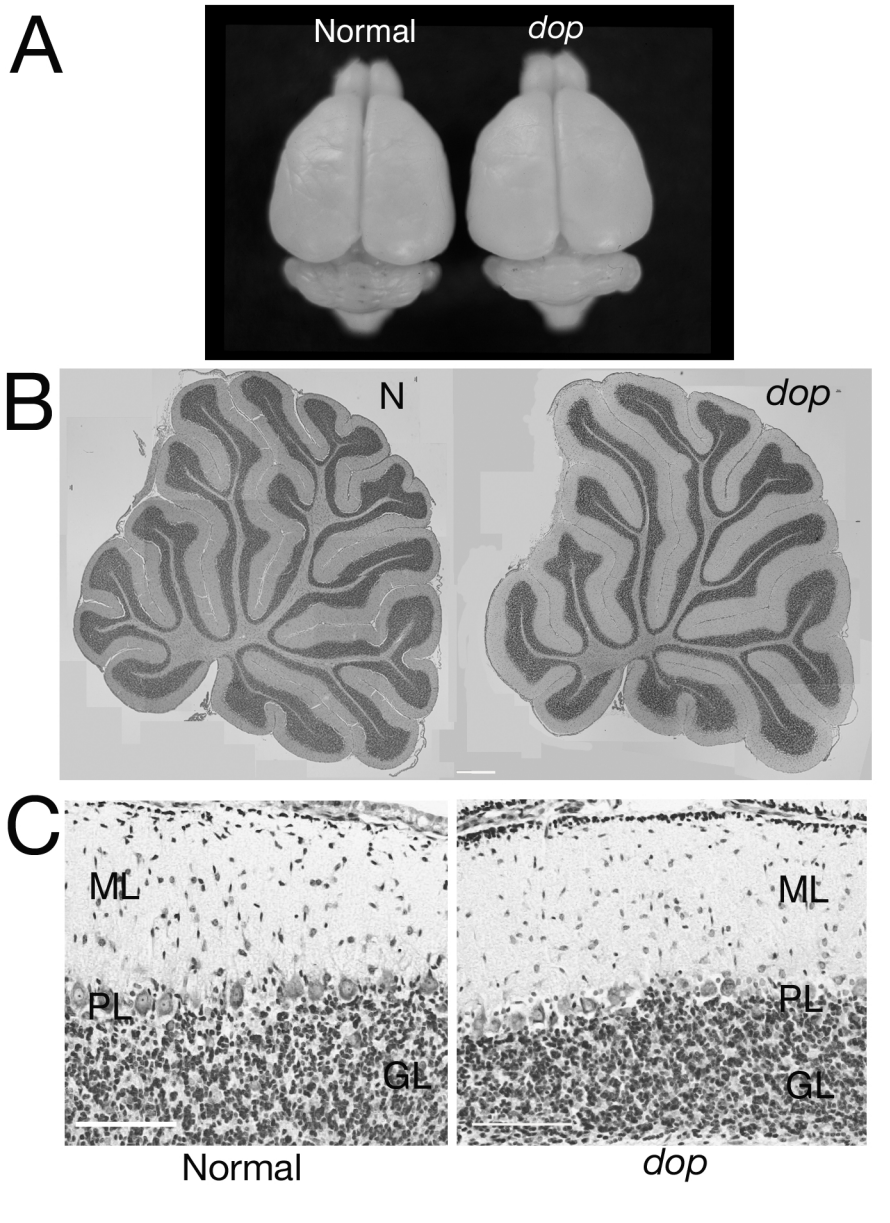

Fig.5

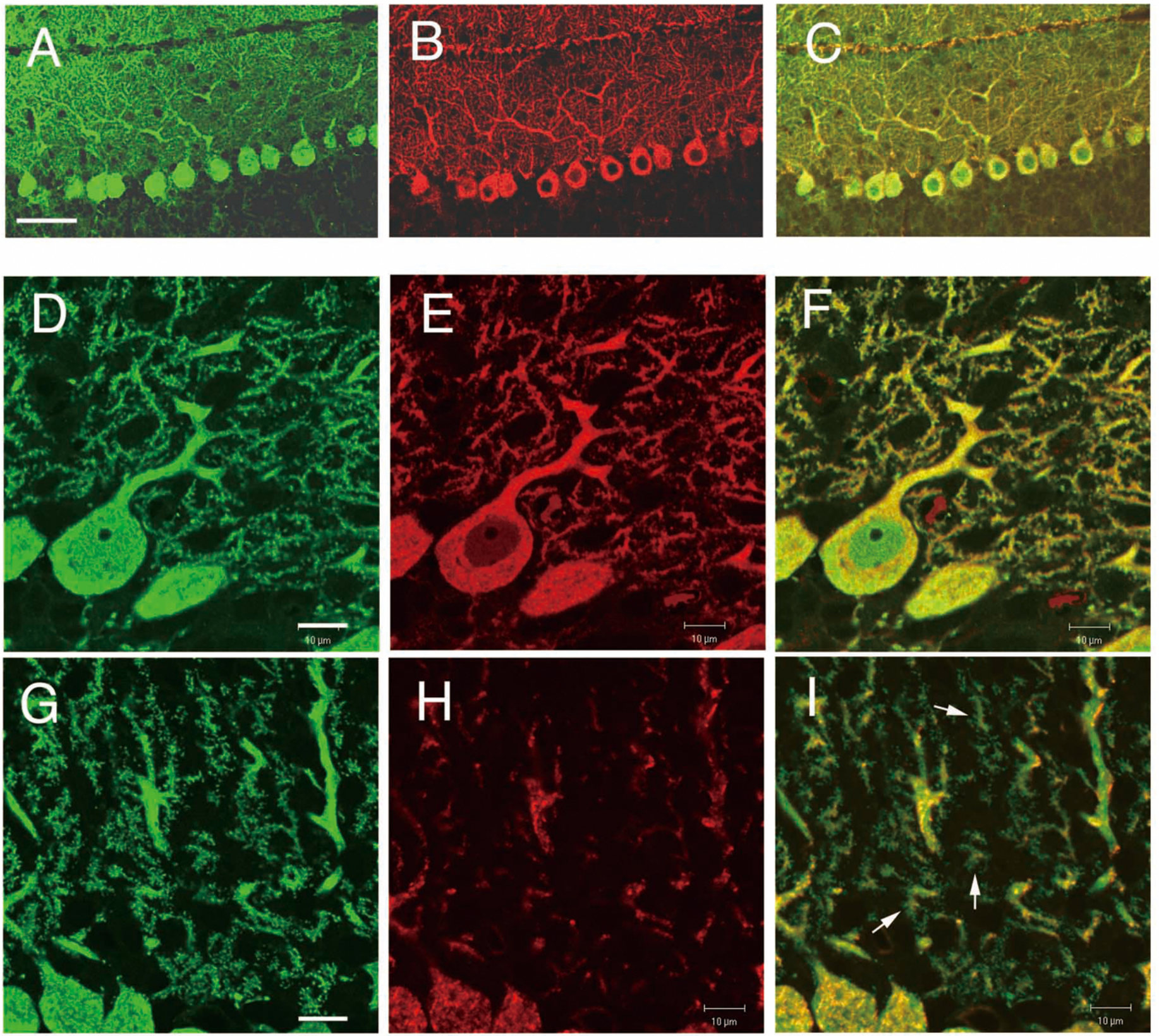

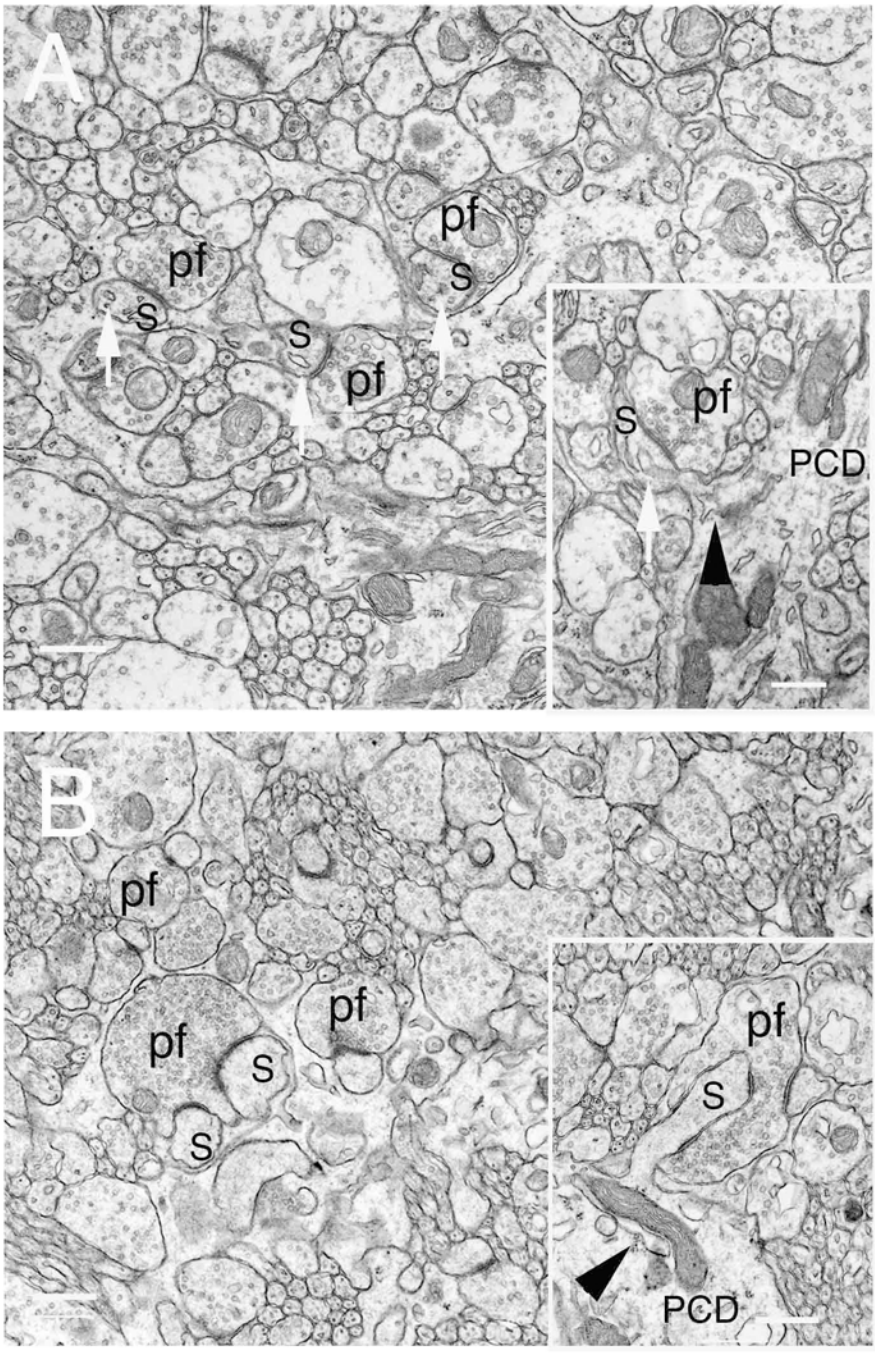
A
pf
pf
s
s
s
pf
pf
s
s
pf
PCD
B
pf
pf
pf
pf
s
s
pf
s
PCD

A

control

pre

25 min

B

mutant

25 min

pre

5 mV

5 ms

C

control

mutant

rats

PF+CF

PF+CF

Normalized EPSP slope

1.5

1.0

0.5

0

-10

0

10

20

30

40

Time (min)

D

mice

PF+CF

PF+CF

Normalized EPSP slope

1.5

1.0

0.5

0

-10

0

10

20

30

Time (min)

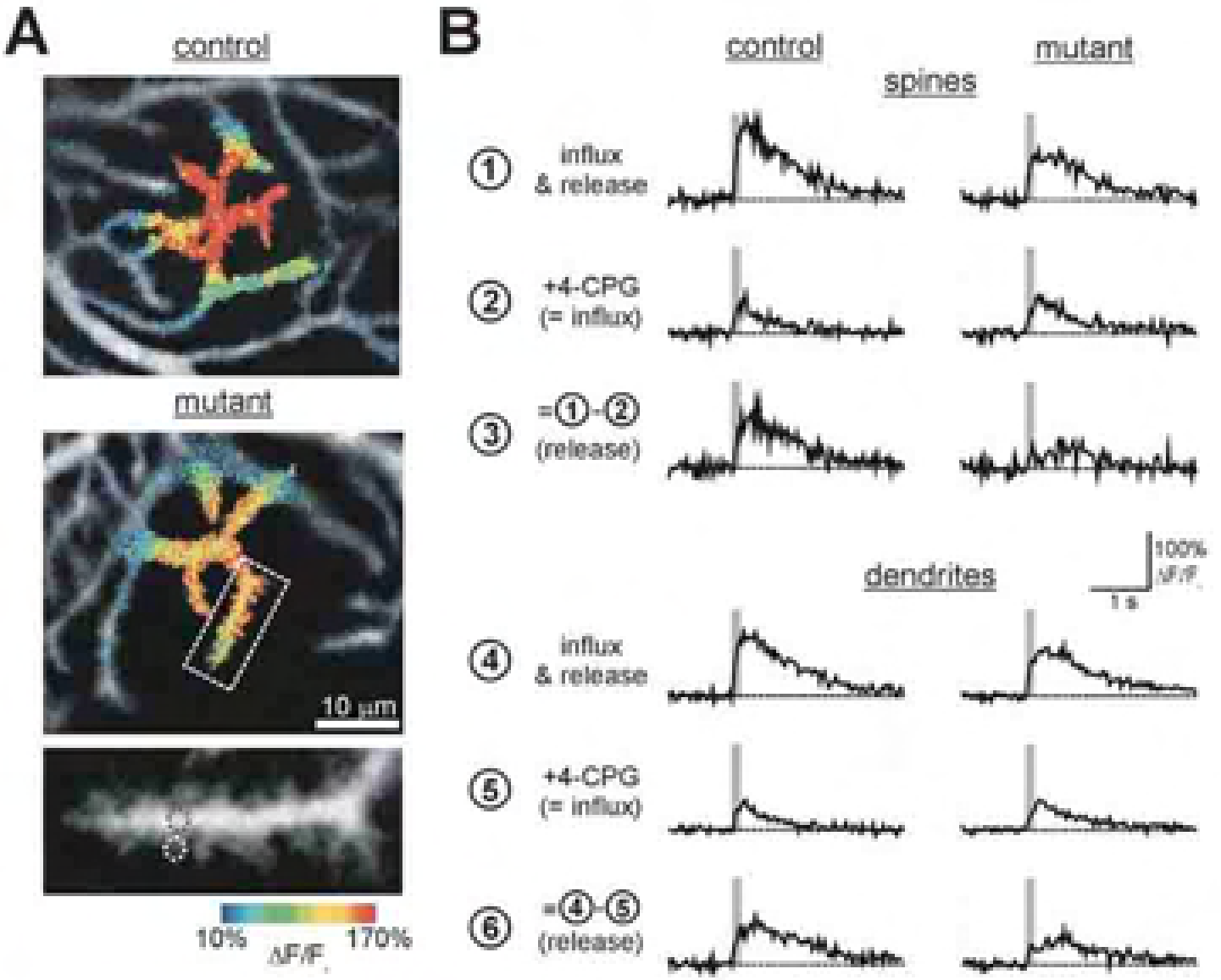
A
control
mutant
10 µm
10%
ΔF/F
170%
B
control
mutant
spines
① influx & release
② +4-CPG (= influx)
③ =①-② (release)
dendrites
100% ΔF/F
1 s
④ influx & release
⑤ +4-CPG (= influx)
⑥ =④-⑤ (release)